Measurement and microscopic analysis of the $^{11}B(\vec{p},\vec{p})$ reaction at $E_p = 150$ MeV. I. Inelastic scattering

V. M. Hannen,[1,*] K. Amos,[2] A. M. van den Berg,[1] R. K. Bieber,[1,†] P. K. Deb,[2] F. Ellinghaus,[3,‡] D. Frekers,[3] M. Hagemann,[4] M. N. Harakeh,[1] J. Heyse,[4,§] M. A. de Huu,[1] B. A. M. Krüsemann,[1,‖] S. Rakers,[3] R. Schmidt,[3] S. Y. van der Werf,[1] and H. J. Wörtche[1]

[1]*Kernfysisch Versneller Instituut, Zernikelaan 25, NL-9747 AA Groningen, The Netherlands*

[2]*School of Physics, University of Melbourne, Victoria 3010, Australia*

[3]*Institut für Kernphysik, Westfälische Wilhelms Universität, D-48149 Münster, Germany*

[4]*Vakgroep Subatomaire en Stralingsfysica, Universiteit Gent, B-9000 Gent, Belgium*

(Received 27 November 2002; published 30 May 2003)

Cross sections and analyzing powers for the $^{11}B(\vec{p},p')$ reaction have been measured using a 150-MeV polarized proton beam from the AGOR cyclotron at KVI. For the stronger inelastic transitions, also spin-flip probabilities have been extracted. To predict cross sections and spin observables a microscopic (coordinate space) model of elastic scattering has been used, whereas for inelastic scattering calculations were performed in the distorted-wave approximation. In the model calculations a medium-modified two-nucleon effective interaction was used and nuclear structure information was obtained from shell-model calculations in a complete $(0+2)\hbar\omega$ model space for parity-conserving transitions and a $1\hbar\omega$ shell-model description in the case of parity-changing transitions. With the help of these model calculations, spin-isovector parts of the $M1$ strengths for the negative-parity states at excitation energies of 2.125 MeV ($J^\pi = 1/2^-$), 4.445 MeV ($J^\pi = 5/2^-$), 5.020 MeV ($J^\pi = 3/2^-$), and 8.920 MeV ($J^\pi = 5/2^-$) have been extracted and compared to known Gamow-Teller strengths for the analog transitions to ^{11}C.

DOI: 10.1103/PhysRevC.67.054320 PACS number(s): 25.40.Cm, 24.70.+s, 25.40.Ep, 27.20.+n

I. INTRODUCTION

Over the last decades, medium-energy proton scattering has been established as a valuable tool for the study of nuclear structure in general and the study of spin-isospin excitations in nuclei in particular [1–4]. The latter makes use of the energy and momentum-transfer dependence of the different spin-flip and non-spin-flip parts of the effective interaction between the incoming proton and the target nucleus [5], which, especially in the energy range between 140 and 400 MeV and under forward scattering angles, results in an enhanced sensitivity to spin-isospin transitions. This selectivity for a certain mode of excitation has also been exploited in this work to study the spin-isovector parts of the $M1$ strengths for transitions to low-lying states in the odd-A nucleus ^{11}B.

As described by Raghavan *et al.* [6–8], the ^{11}B isotope can be used as target material in experiments aiming at the determination of the flux of high-energy ^8B decay neutrinos that are produced during the proton-proton fusion chain in the center of the sun. In the proposed setup, neutrinos can simultaneously be observed via neutral-current (NC) excitation of nuclear levels in ^{11}B and the subsequent detection of γ rays emitted by the deexciting nucleus or via charged-current (CC) scattering of electron neutrinos to states in its mirror nucleus ^{11}C which are then detected by a coincidence of the electron produced in the reaction and γ rays emitted during deexcitation:

$$\mathrm{NC}, \nu + {}^{11}\mathrm{B} \rightarrow \nu' + {}^{11}\mathrm{B}^* \rightarrow \nu' + \gamma + {}^{11}\mathrm{B}, \tag{1}$$

$$\mathrm{CC}, \nu_e + {}^{11}\mathrm{B} \rightarrow e^- + {}^{11}\mathrm{C}^* \rightarrow e^- + \gamma + {}^{11}\mathrm{C}. \tag{2}$$

This detection scheme allows one to measure the total (flavor independent) neutrino flux and the electron-neutrino flux simultaneously and in the same experimental setup.

The extraction of neutrino fluxes from count rates requires a knowledge of the NC excitation strengths λ_{NC} and the CC excitation strengths λ_{CC}. The charged-current excitation strength is given by [7,9]

$$\lambda_{\mathrm{CC}} = B(F) + \left(\frac{g_A}{g_V}\right)^2 B(GT) = \frac{6147 \pm 7}{ft}, \tag{3}$$

where $g_A/g_V = 1.264 \pm 0.002$ [10] is the axial-vector to vector coupling ratio, $B(F)$ is the Fermi transition strength and $B(GT)$ the Gamow-Teller transition strength. For the ground-state transition $^{11}B \rightarrow {}^{11}C$ the log ft value is known: $\ln ft = 3.6$ [11], and the resulting CC excitation strength is $\lambda_{\mathrm{CC}} = 1.54$. The transitions to excited states in ^{11}C are dominantly of Gamow-Teller type and $B(GT)$ strengths for these states have been measured by Taddeucci *et al.* [12] and Grimes *et al.* [13]. In standard electroweak theory, at low momentum transfers, NC excitations proceed only by the isovector axial-vector current [14] and the excitation

*Present address: SRON, Sorbonnelaan 2, 3584 CA Utrecht, The Netherlands. Electronic address: v.m.hannen@sron.nl

†Present address: Universität Köln, Köln, Germany.

‡Present address: DESY, Zeuthen, Germany.

§Present address: EC, JRC, IRMM, Geel, Belgium.

‖Present address: ASF Thomas Industries GmbH & Co. KG, Wuppertal, Germany.

strengths can be derived from measured spin-isovector parts of the $M1$ strengths $B(\sigma\tau_z)\uparrow$ using

$$\lambda_{\mathrm{NC}}=\left(\frac{g_A}{g_V}\right)^2\frac{4\pi}{3}\left(\frac{2}{g_p^s-g_n^s}\right)^2 B(\sigma\tau_z)\uparrow, \tag{4}$$

where $g_p^s=5.586$ and $g_n^s=-3.826$ are the proton and neutron spin g factors, respectively. According to Ref. [6], the NC and CC excitation strengths are connected by a simple proportionality $4\lambda_{\mathrm{NC}}=\lambda_{\mathrm{CC}}$. Effects such as meson-exchange currents (MECs) [15,16] might, however, modify this relation.

Raghavan and Pakvasa [7] used input from shell-model calculations to extract $B(\sigma\tau_z)\uparrow$ values for the levels in question from measured radiative widths [11]. The systematic uncertainties inherent to this approach and the discrepancies that arise when the $B(\sigma\tau_z)\uparrow$ strengths extracted this way are compared to measured Gamow-Teller strengths, make it desirable to obtain information on the spin-isovector parts of the $M1$ strengths from another, independent experimental technique. Because of its selectivity for spin-isospin excitations, medium-energy inelastic proton scattering offers such an opportunity.

In this paper we present results of a study of inelastic excitation of ^{11}B using a polarized proton beam at an incident energy of 150 MeV. In Sec. II, the experimental procedure will be described and the obtained results will be compared to other available data. The calculations used to describe the data will be presented in Sec. III and an interpretation of our data will be discussed in Sec. IV. A summary and conclusion is given in Sec. V. In addition to the study of inelastic transitions, the data also reveal effects of depolarization for elastic scattering. These data and their interpretation will be given in a forthcoming paper [17].

II. EXPERIMENTAL PROCEDURE AND DATA REDUCTION

The experiment was performed at the AGOR facility of the KVI using a 150-MeV polarized proton beam. Scattered particles were momentum analyzed in the Big-Bite Spectrometer (BBS) [18] and detected in the focal-plane detector and focal-plane polarimeter systems built by the EUROSUPERNOVA Collaboration [19]. This detection system consists of three major building blocks: a focal-plane detection system (FPDS), a focal-plane polarimeter (FPP), and a scintillator system. The FPDS consists of two vertical drift chambers (VDC's) mounted parallel to the focal plane of the BBS and separated by 23 cm along the central ray with which they form an angle of 39°. Each chamber has an X plane and a U plane with the wires of the U plane tilted by 32.9° with respect to the vertical direction. The focal-plane polarimeter is located downstream of the FPDS and consists of four multiwire proportional chambers (MWPC's) and a carbon analyzer with a thickness of 5 cm. Each MWPC consists of an X and a Y plane with a wire spacing of 2.5 mm. Event triggers are provided by the scintillator system that consists of two planes with five scintillator paddles in each plane. One of these planes is located before the carbon analyzer and the other one downstream of the last MWPC.

The in-beam polarimeter (IBP), described in Ref. [20], was used to determine the polarization of the proton beams coming from the AGOR cyclotron. It is located in the high-energy beam line leading to the experimental area. The data of this experiment were taken over a period of five days during which the beam polarization was measured roughly three times a day. Each IBP measurement consisted of a run where the transition units and hexapoles of the polarized ion source were turned off to ensure a strictly unpolarized beam [21] and a second run where the three different beam polarizations produced by the ion source were measured. The values for the polarization were $(76\pm2)\%$ for spin up, $(-74\pm2)\%$ for spin down. For the situation where the hexapoles were on, but the transition units were switched off, the remaining polarization in this mode was $(8\pm1)\%$, which we, nevertheless, will denote as "spin off" (cf. Ref. [20], for more details see Ref. [17]).

Data were taken at a number of spectrometer angles in steps of about 2° between 5° and 28° alternately on a 20.1 mg/cm^2 thick self-supporting ^{11}B target with an enrichment of 99.5% [22] and on a 9.0 mg/cm^2 thick natural carbon target. Data from the ^{12}C measurements were used to cross check our experimental results against measurements from groups at other laboratories [23–26] and, therefore, provide a possibility to verify the correct functioning of the detector systems and of the analysis procedure applied in this work. Although no information from the FPP is required to determine cross sections and analyzing powers, the polarimeter was kept running during most of the measurements. The additional data were used to determine spin-flip probabilities for elastic scattering off ^{11}B and for some of the more strongly excited inelastic transitions. The beam from the cyclotron was stopped in a Faraday cup, positioned inside the magnet chambers of the spectrometer at small scattering angles and inside the scattering chamber for large scattering angles ($\Theta_{\mathrm{BBS}}>9°$). The current from the Faraday cup was integrated and, together with the dead time of the data-acquisition system, monitored throughout the experiment.

Using calibration data obtained during a measurement with a sieve slit mounted at the entrance of the spectrometer, the target coordinates δ, ϑ_t, and φ_t were calculated from the focal-plane coordinates of the particles. The angles ϑ_t and φ_t are the horizontal and vertical scattering angles of the particle relative to the central ray through the BBS and δ is the relative magnetic rigidity $\delta=(B\rho-B\rho_0)/(B\rho_0)$, where $B\rho_0$ is the rigidity of the central ray. Using this information, the kinetic energy and the full scattering angle in the laboratory system have been reconstructed. The upper left panel in Fig. 1 shows the horizontal angle ϑ_t plotted against the resulting kinetic energy for 150-MeV protons scattered from ^{11}B at a spectrometer angle $\Theta_{\mathrm{BBS}}=10°$. Vertical lines observed in the plot correspond to states in ^{11}B with the ground state at the highest energy. Events outside the area enclosed between the horizontal dashed lines are rejected to reduce instrumental background. The energy spectrum of the scattered protons is shown in the upper right panel of Fig. 1. The elastic-scattering line, which at this angle is located at an ejectile energy of 149.55 MeV, has been scaled down by a factor 40.

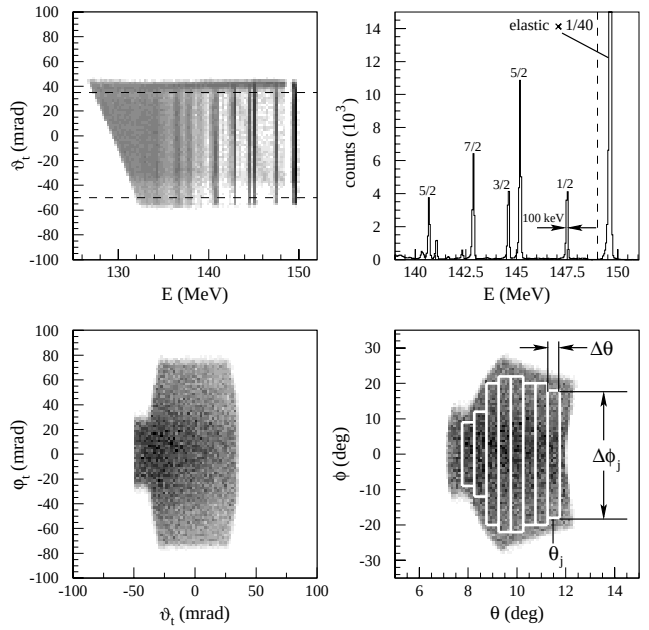

FIG. 1. Plots produced from a measurement in which 150-MeV protons have been scattered from ^{11}B at a spectrometer angle $\Theta_{\mathrm{BBS}}=10°$. The states observed in the upper right panel have been identified using Ref. [11].

The full width at half maximum of the peak at $E_x=2.125$ MeV, which corresponds to the first excited $J^\pi=1/2^-$ state, is about 100 keV. By plotting the vertical target angle φ_t versus the horizontal angle ϑ_t, one obtains an image of the opening of the spectrometer (see Fig. 1, lower left panel). For the determination of the solid angle, however, these angles have been converted into spherical coordinates: the polar and the azimuthal scattering angles θ and ϕ, respectively. By plotting the azimuthal versus the polar angle, one obtains a spherical representation of the BBS opening as shown in the lower right panel of Fig. 1. In this representation the angular acceptance of the spectrometer can be divided easily into strips with a well-defined scattering angle θ_j and solid angle $\Delta\Omega_j=\sin\theta_j\Delta\theta\Delta\phi_j$, as indicated in the figure.

A. Polarized-beam cross section

To extract cross sections from the accumulated data, the counts collected in a certain solid angle bin $\Delta\Omega_j$ and energy bin ΔE_i have to be corrected for the measured dead times of the setup, for the reconstruction efficiency of the VDC's and for the integrated charge. In case of a polarized-beam measurement this must be done separately for each of the polarization states of the beam. For a certain polarization state κ inside the ith energy bin and the jth solid-angle strip, the corrected number of counts per unit charge $C_{\kappa ij}$ then becomes

$$C_{\kappa ij}=\frac{N_{\kappa ij}}{(1-D_\kappa)Q_\kappa\Upsilon}, \tag{5}$$

where $N_{\kappa ij}$ is the uncorrected number of counts, D_κ is the measured dead time of the system, Q_κ is the integrated charge from the beam dump, and Υ is the VDC efficiency that was typically 96%.

A problem that surfaced during data analysis is that the hit density for a fixed scattering angle θ_j decreases when going in the nondispersive plane from the central region of the BBS opening to the upper or lower edge of the acceptance. Quantitatively, the hit density in the central region of the angular acceptance differed by up to 15% from the overall density observed inside a solid-angle strip belonging to a certain scattering angle θ_j. For a proton beam of polarization $\vec{p}_\kappa=(0,p_y^\kappa,0)$, the variation of the cross section due to the analyzing power of a particular nuclear reaction is given by

$$\left.\frac{d\sigma}{d\Omega}(\theta_j,\phi)\right|_\kappa=\left.\frac{d\sigma}{d\Omega}(\theta_j)\right|_0[1+p_y^\kappa\cos\phi A_n(\theta_j)], \tag{6}$$

where $d\sigma/d\Omega(\theta_j)|_0$ is the cross section for an unpolarized beam. The resulting variation in the hit density at a spectrometer angle $\Theta_{\mathrm{BBS}}=5°$ can be estimated, assuming values $p_y=0.7$, $A_n(5°)=0.36$ (corresponding to the analyzing power of elastic scattering from ^{12}C, see Fig. 3, right panel), and an azimuthal coverage of $|\phi|\leqslant 40°$, to be about 4%. At larger spectrometer angles the effect due to the analyzing power becomes smaller because of the decreasing azimuthal coverage of the BBS. For instance, at $\Theta_{\mathrm{BBS}}=21°$, where the analyzing power of the elastic scattering reaches its maximum value of $A_n\approx 0.9$ and $|\phi|\leqslant 11°$, the effect is only about 2%. The experimentally observed variations can, therefore, not be explained by the reaction mechanism, but must have an instrumental origin, most likely caused by an inefficiency of some of the scintillator paddles, during this particular experiment. To correct for the effect, an additional factor ξ_j has been introduced, defined by the ratio of the central to the overall hit density inside a certain solid angle strip, such that the corrected number of counts per unit charge becomes

$$C_{\kappa ij}=\frac{N_{\kappa ij}\xi_j}{(1-D_\kappa)Q_\kappa\Upsilon}. \tag{7}$$

Because the factor ξ_j is averaged between the spin-up and spin-down phases of the beam polarization, which have roughly the same magnitude $|p_y|$ but opposite signs, it is ensured that only the instrumental effect is corrected for and not the real physical variation due to the analyzing power $A_n(\theta)$.

Figure 2 shows the kinetic-energy spectrum of the double-differential cross section for 150-MeV polarized protons scattered from ^{11}B at $\Theta_{\mathrm{BBS}}=10°$. To extract angular distributions of cross sections and analyzing powers of the observed states, the energy spectra at each angle θ_j and polarization $\vec{p}_\kappa$ were fitted using the code FIT [27]. The line shape is approximated by a Gaussian with an exponential tail towards lower energies. The area under the lth peak in a spectrum corresponds to the differential cross section of a certain excited state at the scattering angle and beam polarization at which the spectrum was taken and will be referred to as $d\sigma/d\Omega(\theta_j)|_\kappa^l$.

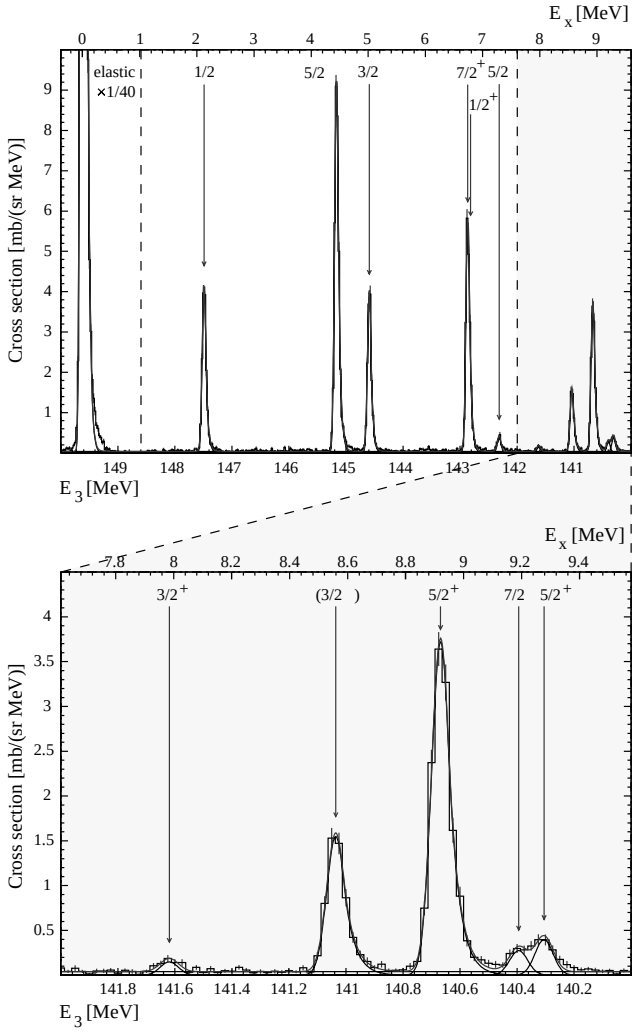

FIG. 2. Double-differential cross section of the reaction $^{11}\mathrm{B}(\vec{p},p')^{11}\mathrm{B}$ at $\Theta_{\mathrm{BBS}}=10°$ as a function of the kinetic energy of the ejectiles. At the top of each panel, the scale for the excitation energy in ^{11}B is given. Experimental data are represented by histograms while the solid lines result from a fitting procedure as described in the text. The spin assignments of the states have been taken from Ref. [11].

B. Analyzing power and unpolarized-beam cross section

The analyzing power $A_n(\theta)$ of a particular nuclear reaction can be determined by performing measurements with different beam polarizations p_y^1 and p_y^2. Dividing the cross sections given by Eq. (6) for the two polarization states, one obtains

$$\left.\frac{d\sigma}{d\Omega}(\theta_j,\phi)\right|_1^l \Big/ \left.\frac{d\sigma}{d\Omega}(\theta_j,\phi)\right|_2^l = \frac{1+p_y^1\cos\phi A_n(\theta_j)}{1+p_y^2\cos\phi A_n(\theta_j)}, \tag{8}$$

which, when averaging over the azimuthal interval $\Delta\phi_j$, results in

$$\left.\frac{d\sigma}{d\Omega}(\theta_j)\right|_1^l \Big/ \left.\frac{d\sigma}{d\Omega}(\theta_j)\right|_2^l = \frac{1+p_y^1\langle\cos\phi\rangle_j A_n(\theta_j)}{1+p_y^2\langle\cos\phi\rangle_j A_n(\theta_j)} \tag{9}$$

with

$$\langle\cos\phi\rangle_j=\frac{1}{\Delta\phi_j}\int_{\Delta\phi_j}\cos\phi d\phi. \tag{10}$$

Solving Eq. (9) for $A_n(\theta_j)$, one gets

$$A_n(\theta_j)=\frac{\left.\frac{d\sigma}{d\Omega}(\theta_j)\right|_1^l-\left.\frac{d\sigma}{d\Omega}(\theta_j)\right|_2^l}{\left.\frac{d\sigma}{d\Omega}(\theta_j)\right|_2^l p_y^1\langle\cos\phi\rangle_j-\left.\frac{d\sigma}{d\Omega}(\theta_j)\right|_1^l p_y^2\langle\cos\phi\rangle_j}. \tag{11}$$

Once the analyzing power of a particular reaction is known, the unpolarized-beam cross section of that reaction can be calculated from any of the polarized-beam cross sections via

$$\left.\frac{d\sigma}{d\Omega}(\theta_j)\right|_0^l=\frac{\left.\frac{d\sigma}{d\Omega}(\theta_j)\right|_\kappa^l}{1+p_y^\kappa\langle\cos\phi\rangle_j A_n(\theta_j)}. \tag{12}$$

C. Results and comparison with existing data

Angular distributions of cross sections and analyzing powers with center-of-mass angles in the range of $4° \leqslant \theta_{\mathrm{c.m.}} \leqslant 31°$ in the ^{11}B case and $4° \leqslant \theta_{\mathrm{c.m.}} \leqslant 29°$ in the ^{12}C case have been extracted from the data. For ^{11}B, all positive- and negative-parity states [11] up to the $J^\pi=5/2^+$ state at an excitation energy of $E_x=9.274$ MeV have been analyzed with the exception of the $1/2^+$ state at 6.792 MeV. As will be mentioned in Sec. III B, the $B(E2)$ strength for the transition to the $7/2^-$ state at 6.743 MeV is much larger than the $B(E1)$ strength for the transition to this $1/2^+$ state. This is also consistent with the results from Hasselgren *et al.* [28] in their analysis of (p,p') scattering from ^{11}B at a bombarding energy of 185 MeV and with the measured and calculated angular distributions for this peak as presented for this work in Sec. III C. The peak at 6.7 MeV will therefore be treated as the $7/2^-$ state located at $E_x=6.743$ MeV. In case of the negative-parity states, the BBS acceptance has been divided into four 1° bins, while for the weaker positive-parity states the angular bins of a setting were joined to form one 4° bin in order to gain sufficiently high statistics. The overall systematic uncertainty of the measured cross sections, which accounts for errors in dead-time corrections, in the calculation of inefficiencies and acceptances, and in the integrated charges and target thicknesses, is assumed to be about 10%.

A comparison of elastic cross-section and analyzing-power data extracted from the ^{12}C measurements to existing datasets measured in Orsay [24] and at IUCF [26] is shown

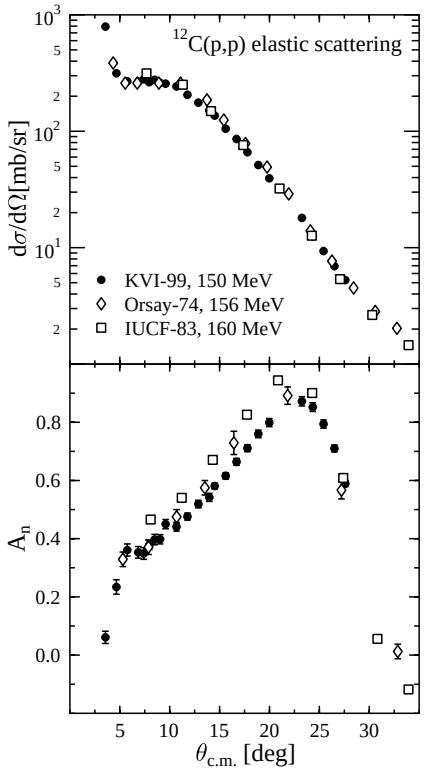

FIG. 3. Differential cross section (upper panel) and analyzing power (lower panel) for elastic scattering of protons from ^{12}C. The Orsay-74 and IUCF-83 datasets have been taken from Refs. [24] and [26], respectively.

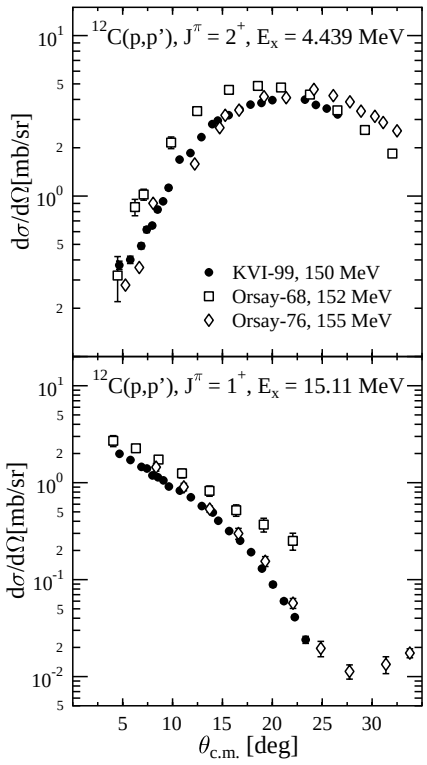

FIG. 4. Differential cross sections for inelastic scattering of protons from ^{12}C to the $J^\pi = 2^+$ state at $E_x = 4.439$ MeV (upper panel) and the $J^\pi = 1^+$ state at $E_x = 15.11$ MeV (lower panel). The Orsay-68 and Orsay-76 datasets have been taken from Refs. [23] and [25], respectively.

in Fig. 3. While there is excellent agreement between the cross sections observed at the different laboratories, the analyzing power measured at IUCF at an incoming proton energy of 160 MeV lies slightly above the data measured at 156 and 150 MeV at Orsay and KVI, respectively. This can be explained by the energy dependence of the elastic-scattering analyzing power in this angular region, which reaches its maximum at about 200 MeV [29]. Figure 4 shows two examples for cross sections of inelastic transitions in ^{12}C. Data taken at KVI are compared to datasets measured in Orsay, one in the late 1960s [23] and one in the mid 1970s [25]. While there is good agreement between the KVI data and the latter measurement, the older Orsay data indicate a substantially higher cross section.

Figure 5 shows the results for elastic scattering on ^{11}B compared to the only other available elastic-scattering dataset obtained near our bombarding energy, which has been measured at Orsay [30]. There is good agreement between the analyzing powers of the measurements, while the cross sections at smaller angles differ substantially.

For the inelastic transitions there are two more datasets at an incoming proton energy of 185 MeV, both measured at Uppsala [28,31], which can be used to compare with our data. Figure 6 shows measured cross sections for a number of negative-parity states in ^{11}B as a function of the transferred momentum q. This representation allows an easier comparison of datasets at different incoming proton energies. While there is agreement between the KVI data and the Uppsala measurements for some of the states and momentum transfers, the older measurements generally yield higher cross sections for the analyzed states. Two experimental circumstances may play a role in this respect. First, the older measurements suffered from a poor energy resolution, which has been 350 to 450 keV in the Uppsala case and 700 to 800 keV during the Orsay experiments. This makes it difficult to separate some of the states, for instance in the case of the $5/2^-$ state at 8.920 MeV and the two nearby positive-parity states at 9.185 and 9.274 MeV, which are observed as one peak. Second, in contrast to the KVI experiment where a self-supporting boron target was used, the older measurements were performed using pressed powder targets enclosed between aluminum or mylar foils. Protons scattered from the additional material cause an instrumental background in the energy spectra, which may not always be easy to separate from the relevant excited states in ^{11}B.

III. CALCULATIONS

We will now describe the results of model calculations that have been performed to reproduce the measured differential cross sections, analyzing powers, and spin-flip probabilities. The main ingredients of the calculations, namely, the effective nucleon-nucleon interaction and the shell-model wave functions, were tested by comparing calculated results to measured elastic cross sections and electromagnetic transition strengths (see Secs. III A and III B, respectively).

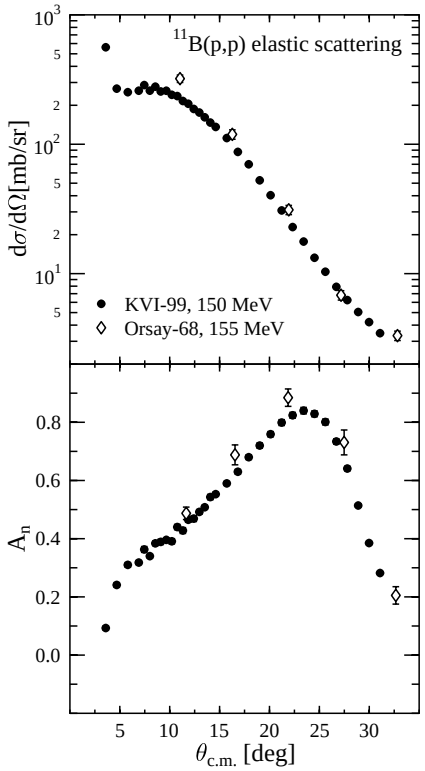

FIG. 5. Differential cross section (upper panel) and analyzing power (lower panel) for elastic scattering of protons from ^{11}B. The Orsay-68 dataset has been taken from Ref. [30].

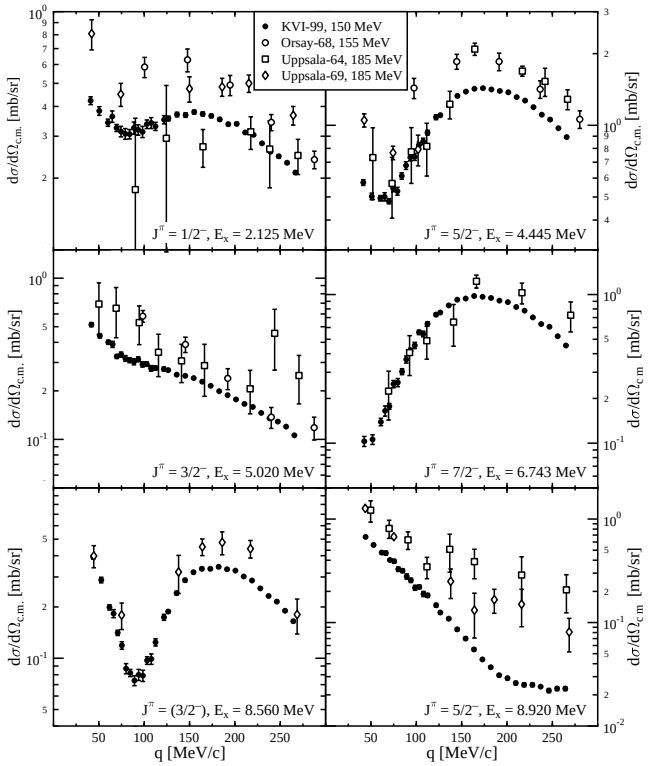

FIG. 6. Differential cross sections for inelastic scattering of protons from ^{11}B to several low-lying states. The Orsay-68, Uppsala-64, and Uppsala-69 datasets have been taken from Refs. [30,28,31], respectively. Excitation energies and spin assignments have been taken from Ref. [11].

A. Choice of the effective nucleon-nucleon interaction

Several effective nucleon-nucleon interactions have been tested by comparing elastic scattering cross sections and analyzing powers calculated using a microscopic folding optical potential to experimental results. The ^{12}C(p,p) reaction at a proton energy of 150 MeV has been chosen as a test case because, contrary to the ^{11}B(p,p) reaction, no higher multipoles contribute to the elastic scattering cross section. In this case the necessary input from nuclear shell-model calculations is limited to the specification of the ground-state density matrix of the target nucleus. The optical potential has been generated by folding the effective interaction with the ground-state density matrix (for details see, e.g., Ref. [32]). Occupation numbers of the single-particle states can be calculated in a $0\hbar\omega$ model space using the OXBASH shell-model code [33]. The resulting average number of particles in each orbit is: $1s_{1/2}=2$, $1p_{3/2}=3.267$, and $1p_{1/2}=0.733$ and it is equal for protons and neutrons. Occupation numbers obtained in a complete $(0+2)\hbar\omega$ model space have also been tested, but did not produce a significant difference in the results obtained using a microscopic folding optical potential. The single-particle wave functions were calculated using a harmonic oscillator potential. The range parameter b of this potential can be estimated from the root-mean-square charge radius $(\langle r^2\rangle)^{1/2}$ of the nucleus using [34]

$$(\langle r^2\rangle)^{1/2}=b\sqrt{\frac{5Z-4}{2Z}}. \tag{13}$$

For ^{12}C a radius of 2.47 fm has been assumed [35] leading to $b=1.68$ fm.

Four different effective interactions were used in the calculations. As an example of a free t-matrix interaction, the parametrization of Franey and Love [36], which has been extensively used in the analysis of proton-scattering experiments, has been chosen. Another approach is based on g-matrix type interactions, which include medium effects in the description of the nucleon-nucleon scattering. These have, among others, been provided by Von Geramb [37], Nakayama and Love [38], and by the Melbourne group; see, e.g., Dortmans and Amos [39]. The most recent of these medium-modified interactions is the one provided by the Melbourne group. It has been shown to perform well on a large number of target nuclei [40] and over a wide range of incoming proton energies [29]. As shown in Fig. 7, the Melbourne interaction yields a very close description of the shape of the differential cross section while overestimating its magnitude by about 20% for scattering angles $\theta_{c.m.}\leqslant 30°$. In contrast, the other interactions overestimate the measured cross section by up to a factor of 2, especially towards smaller angles. In case of the analyzing power the best agreement is obtained using Von Geramb's interaction. Generally speaking, the medium-modified interactions result in a closer description of the data than the free t-matrix parametrization of Franey and Love.

Because the use of the Melbourne interaction results in

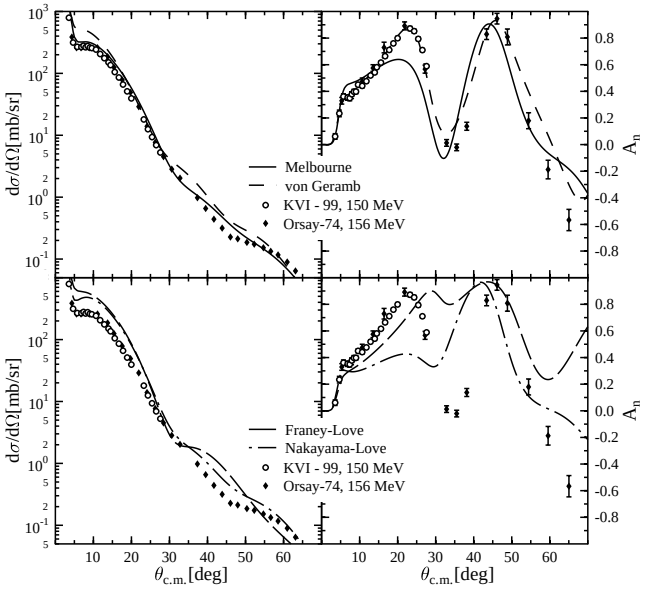

FIG. 7. Microscopic calculations of the differential cross section and analyzing power for elastic scattering of 150-MeV protons from ^{12}C compared to the experimental results. The ''Orsay-74'' dataset is taken from Ref. [24].

the closest reproduction of the shape and magnitude of the differential cross section, which is important when trying to extract transition strengths from the data, it will be used for all distorted-wave Born approximation DWBA) calculations presented in the following sections.

B. Choice of the model space

Microscopic distorted-wave calculations of inelastic transitions or of higher multipole contributions to elastic scattering require one-body transition densities that can be obtained from the nuclear shell model. The shell-model calculations presented here were performed using the OXBASH code [33], which comes with a wide variety of parametrizations of the residual nucleon-nucleon interaction for different configuration spaces. To find out which of these parametrizations result in a suitable description of the transitions in question, electromagnetic transition strengths calculated from the model wave functions are compared to results from (e,e') or γ-decay measurements available in the literature [11,41]. Because of the different configuration spaces required for the description of transitions to negative- or positive-parity states, these two cases will be investigated separately.

1. Parity-conserving transitions

Parity-conserving transitions can be described in a simple $0\hbar\omega$ model space using the parametrizations of the residual interaction provided by Cohen and Kurath [42]. A more realistic description, especially of electric quadrupole transitions, can be obtained by extending the model space to a $(0+2)\hbar\omega$ configuration.

The different parametrizations are referred to by labels CKII for the $0\hbar\omega$ and MK3W for the $(0+2)\hbar\omega$ model space. The CKII interaction is identical to the $(8-16)$2BME interaction from Ref. [42] while the MK3W interaction is constructed from a number of different parametrizations of the residual interaction for each of the participating subshells. The latter interaction has been applied successfully to the analysis of inelastic proton scattering from ^{12}C [43]. Table I gives an overview of measured $B(O\lambda)$ values [11] versus results of the two different shell-model calculations. Bare g factors and free charges were used in the calculations. The radial matrix elements were computed using harmonic-oscillator wave functions with $b=1.69$ fm (obtained from Ref. [35]). Generally, there is a poor agreement between measured and calculated transition strengths. For the $B(M1)$ values both calculations yield similar results, while the $B(E2)$ strengths are better reproduced in the larger model space. The one-body transition densities used for the DWBA calculations of parity-conserving transitions are therefore calculated using the MK3W interaction.

TABLE I. Experimental $B(O\lambda)$ values for parity-conserving transitions in ^{11}B $[J^\pi(\text{g.s.})=3/2^-]$ from Ref. [11] compared to OXBASH results. Units are $e^2\text{fm}^{2\lambda}$ for $B(E\lambda)$ values and $\mu_N^2\text{fm}^{2\lambda-2}$ for $B(M\lambda)$ values.

E_x (MeV)	J^π	$O\lambda$	$B(O\lambda)\uparrow_{expt}$	$B(O\lambda)\uparrow_{SM}$ CKII $0\hbar\omega$	$B(O\lambda)\uparrow_{SM}$ MK3W $(0+2)\hbar\omega$
2.125	$1/2^-$	$M1$	0.54 ± 0.04	0.94	1.10
		$E2$	2.6 ± 0.4	0.88	1.50
4.445	$5/2^-$	$M1$	0.80 ± 0.03	0.78	0.67
		$E2$	21.3 ± 5.30	8.91	16.0
5.020	$3/2^-$	$M1$	1.15 ± 0.04	1.38	1.18
6.743	$7/2^-$	$E2$	3.7 ± 0.9	1.08	3.68
8.920	$5/2^-$	$M1$	0.749 ± 0.004	0.49	0.361
		$E2$	1.6 ± 1.2	0.0003	0.042

2. Parity-changing transitions

Transitions to positive-parity states in ^{11}B require calculations in at least a $1\hbar\omega$ model space, allowing for the excitation of nucleons from the $1s$ to the $1p$ and from the $1p$ to the $2s$ and $1d$ shells. A suitable parametrization of the residual interaction in this model space is the SPSDMWK interaction, which, like the MK3W interaction, is constructed from a number of other parametrizations. The MK3W interaction itself may also be used and allows, in a restricted way, also for $3\hbar\omega$-type excitations. The results of the two types of shell-model calculations are compared to experimental $B(O\lambda)$ values from Ref. [41] in Table II. As for the parity-conserving transitions, the matrix elements were calculated with bare g factors and free charges. Except for the positive-parity states at $E_x=9.185$ MeV and $E_x=9.274$ MeV the SPSDMWK interaction produces better results and is, therefore, used in the DWBA calculations of parity-changing transitions in Sec. III C 2.

C. Inelastic scattering from ^{11}B

Because of its nonzero ground state spin $J^\pi=3/2^-$ and isospin $T=1/2$, inelastic transitions to states within ^{11}B al-

TABLE II. Experimental $B(O\lambda)$ values for parity-changing transitions in ^{11}B from Ref. [41] compared to OXBASH results. Units are $e^2\mathrm{fm}^{2\lambda}$ for $B(E\lambda)$ values and $\mu_N^2\mathrm{fm}^{2\lambda-2}$ for $B(M\lambda)$ values.

E_x (MeV)	J^π	$O\lambda$	$B(O\lambda)\uparrow_{expt}$	$B(O\lambda)\uparrow_{SM}$ SPSDMWK $1\hbar\omega$	MK3W $(1+3)\hbar\omega$
6.792	$1/2^+$	$E1$	$(3.96\pm0.48)\times10^{-4}$	3.51×10^{-4}	1.27×10^{-3}
7.286	$5/2^+$	$E1$	$(3.71\pm0.29)\times10^{-3}$	6.52×10^{-3}	1.20×10^{-2}
7.978	$3/2^+$	$E1$	$(1.00\pm0.13)\times10^{-3}$	4.12×10^{-3}	8.16×10^{-3}
9.185	$7/2^+$	$M2$	9.3 ± 4.1	3.32	10.61
9.274	$5/2^+$	$E1$	$(9.6\pm1.9)\times10^{-4}$	1.55×10^{-2}	3.05×10^{-3}

ways consist of at least two different multipole contributions ΔJ which, in turn, are made up of a number of possible combinations of orbital momentum transfer ΔL, spin transfer ΔS, and isospin transfer ΔT. The allowed $JLST$ combinations follow the usual selection rules for angular momentum coupling with the additional restriction that the orbital momentum transfer ΔL has to be even for parity-conserving transitions and odd for parity-changing transitions. Table III gives an overview of the allowed $JLST$ combinations for transitions to the first excited negative- and positive-parity states in ^{11}B.

The calculated contribution of a particular J transfer to a certain transition depends on the shell-model wave functions of the initial and final states and on the relevant parts of the effective nucleon-nucleon interaction. The total cross section is given by an incoherent sum over the cross sections of the different multipole contributions

$$\frac{d\sigma}{d\Omega}=\sum_{\Delta J}\left(\frac{d\sigma}{d\Omega}\right)_{\Delta J} \tag{14}$$

and the analyzing power and spin-flip probability are given by

$$A_n=\left(\frac{d\sigma}{d\Omega}\right)^{-1}\sum_{\Delta J}(A_n)_{\Delta J}\left(\frac{d\sigma}{d\Omega}\right)_{\Delta J}, \tag{15}$$

TABLE III. Examples of allowed $JLST$ combinations for parity-conserving transitions and parity-changing transitions in ^{11}B.

	$J_i^\pi=3/2^-\rightarrow J_f^\pi=1/2^-$			
Type	ΔJ	ΔL	ΔS	ΔT
$M1$	1	0	1	0
	1	0	1	1
	1	2	1	0
	1	2	1	1
$E2$	2	2	0	0
	2	2	0	1
	2	2	1	0
	2	2	1	1
$E1$	1	1	0	0
	1	1	0	1
	1	1	1	0
	1	1	1	1
$M2$	2	1	1	0
	2	1	1	1
	2	3	1	0
	2	3	1	1

$$S_{nn'}=\left(\frac{d\sigma}{d\Omega}\right)^{-1}\sum_{\Delta J}(S_{nn'})_{\Delta J}\left(\frac{d\sigma}{d\Omega}\right)_{\Delta J}. \tag{16}$$

Because of the poor reproduction of experimentally observed transition strengths by the shell-model calculations (see Tables I and II) the magnitudes of the different multipole contributions to the measured cross sections may not be predicted correctly by the DWBA calculations. If the multipole parts of a certain transition are renormalized to fit the observed cross section, the resulting scaling factors can be used to estimate corrections to the calculated transition strengths (see Sec. IV).

Table IV gives an overview of allowed multipole contributions to the observed transitions and the scaling factors extracted in the analysis. The experimental data and the fits obtained from microscopic DWBA calculations of negative-

TABLE IV. Scaling factors obtained by fitting calculated multipole contributions to measured differential cross sections. The systematic error of the quoted numbers is about 20% unless a range of values is given for a certain scaling factor. The abbreviation ''n.c.'' means that the particular J transfer gives no significant contribution to the observed cross sections.

E_x (MeV)	J^π	$\Delta J=0$	$\Delta J=1$	$\Delta J=2$	$\Delta J=3$	$\Delta J=4$	$\Delta J=5$
2.125	$1/2^-$		0.3	0.7			
4.445	$5/2^-$		0.5	0.75	n.c.	n.c.	
5.020	$3/2^-$	n.c.	0.47	0.3	0.6		
6.743	$7/2^-$			0.7	n.c.	n.c.	n.c.
8.920	$5/2^-$		1.2	0.5	n.c.	n.c.	
7.286	$5/2^+$		0.1–1	0.2–0.3	0.7	$\leqslant0.3$	
7.978	$3/2^+$	$\leqslant1$	$\leqslant0.5$	n.c.	$\leqslant0.8$		
9.185	$7/2^+$			0.5	0.5	n.c.	n.c.
9.274	$5/2^+$		$\leqslant0.4$	n.c.	3−4	n.c.	

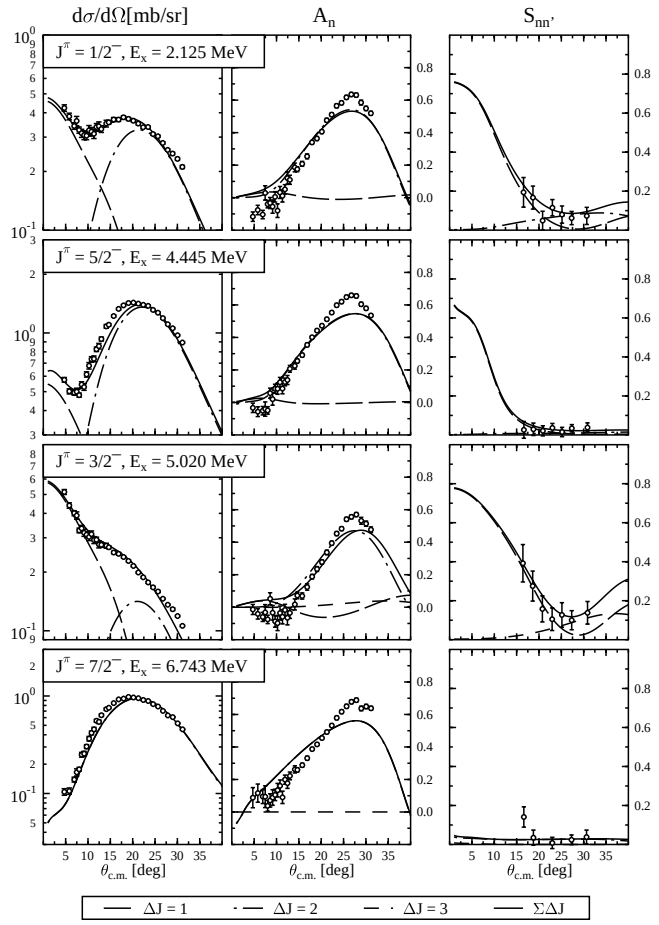

FIG. 8. Transitions to the first four negative-parity states in ^{11}B. Only J transfers that give a significant contribution to the observed angular distributions are plotted. Excitation energies and spin assignments have been taken from Ref. [11].

and positive-parity states, using the DWBA98 code [44] and the microscopic wave functions mentioned above, will be discussed in the following paragraphs.

1. Negative-parity states

Figures 8 and 9 display the measured angular distributions of cross sections, analyzing powers, and spin-flip probabilities for the negative-parity states together with fits obtained from the calculated multipole contributions to each state. The experimental values for the spin-flip probability $S_{nn'}$ have been corrected for a small systematic offset, as discussed in Ref. [17].

The magnitudes of the multipole contributions to a certain state were fixed by a ''fit-by-eye'' procedure to the observed cross section. There were two reasons not to use an automatic least χ^2-fit routine for the fit. First, the focus of the analysis is on the extraction of $M1$ strengths from the data and it is therefore necessary to get a good description of the data points at the most forward scattering angles, while an automatic fit weighs the data points by their statistical errors only. Second, the manual procedure allows us to take into account the additional information provided by analyzing powers and spin-flip probabilities in cases where there is an

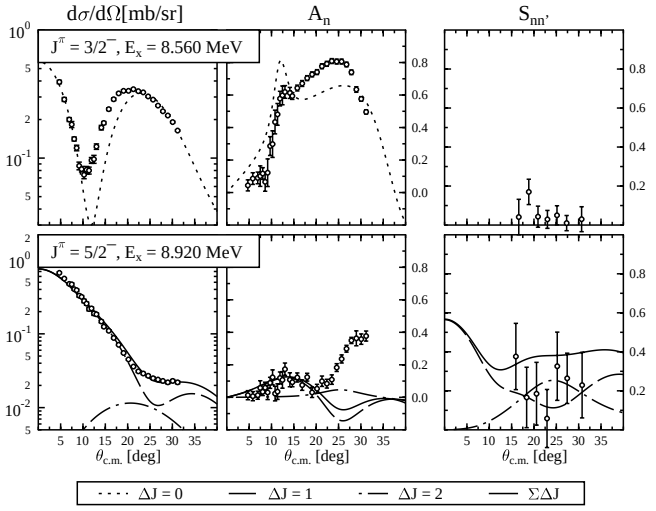

FIG. 9. Same as Fig. 8, but in this case for transitions to the negative-parity states at $E_x = 8.560$ and $E_x = 8.920$ MeV in ^{11}B.

ambiguity in the fit of the cross section data. We estimate the uncertainty of the fitting procedure to be about 10%. Together with the systematic uncertainty of the measured cross sections (see Sec. II C) the error on the resulting scaling factors displayed in Table IV is about 20%.

Over the observed angular region, the cross sections of most of the negative-parity states are governed exclusively by the $M1$ and $E2$ parts of the transitions. In case of the $J^\pi = 3/2^-$ state at $E_x = 5.02$ MeV it was possible to fix also the $\Delta J = 3$ part which gives a significant contribution to the spin-flip probability at larger angles. It is seen from Fig. 8 that indeed the state at $E_x = 7.6$ MeV shows an angular distribution that can be described by a pure $\Delta J = 2$ transition, supporting the assumption that this peak is the $J^\pi = 7/2^-$ state located at 6.743 MeV.

A special case is the state at $E_x = 8.56$ MeV for which Ajzenberg-Selove gives a tentative assignment of $J^\pi = 3/2^-$ [11]. The steep rise of the cross section towards small angles indicates that the transition is predominantly of $E0$ type. Because the shell-model calculations presented here do not produce a theoretical candidate for this state (see also Ref. [45]), one-body-transition densities that have been calculated for a $0^+ \rightarrow 0^+$ transition in ^{12}C have been used to produce angular distributions of a pure $E0$ transition. As can be seen in the upper part of Fig. 9, the shapes of the resulting curves are in good agreement both with the experimentally observed cross section and the analyzing power. The assumption that the transition is governed by the $\Delta J = 0$ contribution and the assignment of a $J^\pi = 3/2^-$ spin and parity to the state is therefore confirmed.

2. Positive-parity states

The good energy resolution and high statistics of the data presented in this work made it possible to observe for the first time positive-parity states in ^{11}B using inelastic proton scattering. Because the parity-changing transitions are much weaker than those excitations that conserve parity, the ex-

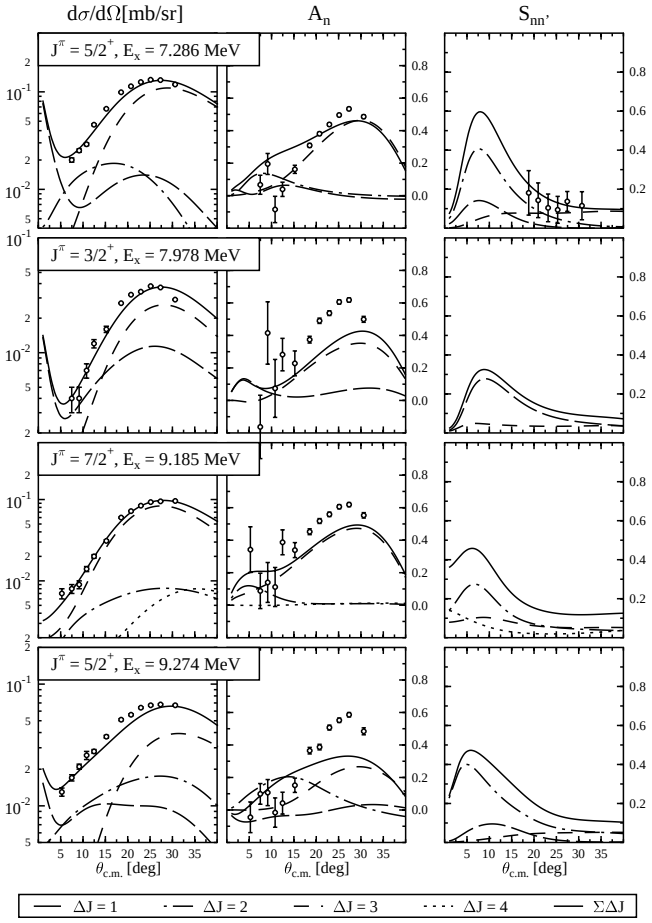

FIG. 10. Same as Fig. 8, but in this case for transitions to positive-parity states in ^{11}B.

traction of the spin-flip probability was only feasible for the strongest of the four observed positive-parity states, i.e., the state at $E_x = 7.286$ MeV.

Figure 10 displays results of the analysis together with fits from the DWBA calculations. Compared to the parity-conserving transitions, more of the possible J transfers to a certain state play a role in the observed angular region. This makes it impossible to obtain an unambiguous determination of the magnitudes of the multipole contributions for a transition. Therefore, most of the scaling factors listed in Table IV are given as a range or a limit on the contribution of a certain multipolarity to a state and the fits displayed in Fig. 10 have to be regarded as examples for possible descriptions of the measured angular distributions. For a clear determination of the multipole contributions to transitions to positive-parity states in ^{11}B, experimental data over a wider angular range than covered in this experiment are required.

IV. DISCUSSION

The main interest in the present work lies in the extraction of the spin-isovector parts of the $M1$ strengths for transitions to low-lying negative-parity states in ^{11}B. Because of the number of possible combinations of orbital momentum transfer, spin transfer, and isospin transfer, which contribute to each transition in ^{11}B (see Table III), the extraction of transition strengths from measured differential cross sections requires additional knowledge of the structure of the transition operators and of the strengths of the terms of the effective nucleon-nucleon interaction corresponding to the different parts of these operators. In the following sections $M1$ and $E2$ type transitions to negative-parity states in ^{11}B will be investigated and arguments will be given as to which parts of the respective operators dominate these transitions. In Sec. IV B, extracted spin-isovector parts of the $M1$ transition strengths will be compared to Gamow-Teller strengths obtained from ^{11}B$(p,n)^{11}$C measurements [12,13].

TABLE V. $M1$ transition strengths calculated from shell-model wave functions of selected negative-parity states in ^{11}B using different parts of the $M1$ operator.

E_x (MeV)	J^π	$B(M1)_{full}$ (μ_N^2)	$B(\sigma+\sigma\tau_z)$ (μ_N^2)	$B(\sigma)$ (μ_N^2)	$B(\sigma\tau_z)$ (μ_N^2)
2.125	$1/2^-$	1.10	1.65	0.042	1.17
4.445	$5/2^-$	0.67	1.05	0.022	0.77
5.020	$3/2^-$	1.18	1.35	0.032	0.97
8.920	$5/2^-$	0.36	0.26	0.008	0.36

A. Extraction of $M1$ strengths

It is possible to express the operator for magnetic dipole transitions in terms of isospin-dependent and isospin-independent contributions [46], using

$$O(M1) = \frac{\mu_N}{2} \sum_{k=1}^{A} \{[(1-\tau_{zk})g_p^s + (1+\tau_{zk})g_n^s]\vec{s}_k \quad (17)$$

$$+[(1-\tau_{zk})g_p^l + (1+\tau_{zk})g_n^l]\vec{l}_k\}. \quad (18)$$

Inserting numerical values $g_p^s = 5.586$, $g_n^s = -3.826$, $g_p^l = 1$, and $g_n^l = 0$ for the g factors, transitions strengths for the different components of the $M1$ operator can be calculated from shell-model wave functions (see Sec. III B). Table V gives an overview of transition strengths of selected negative-parity states in ^{11}B calculated by applying either the complete $M1$ operator $[B(M1)_{full}]$, the spin-dependent parts only $[B(\sigma+\sigma\tau_z)]$, or specifically the spin-isoscalar $[B(\sigma)]$ and spin-isovector $[B(\sigma\tau_z)]$ parts of the operator.

To get an insight into the influence of the effective nucleon-nucleon interaction on the nature of the observed $M1$ transitions, the momentum-transfer dependence of the different parts of the interaction has to be known. For this and for further discussion we consider the Love-Franey effective two-nucleon interaction [5], since the medium-modified Melbourne interaction used heretofore is quite complex to display. The Love-Franey components are quite similar though to the zero density elements of the Melbourne force.

The orbital parts of the $M1$ transition density couple only to the spin-orbit parts of the effective interaction [47], denoted as t^{LS} and t_τ^{LS}, respectively. As both of these forces

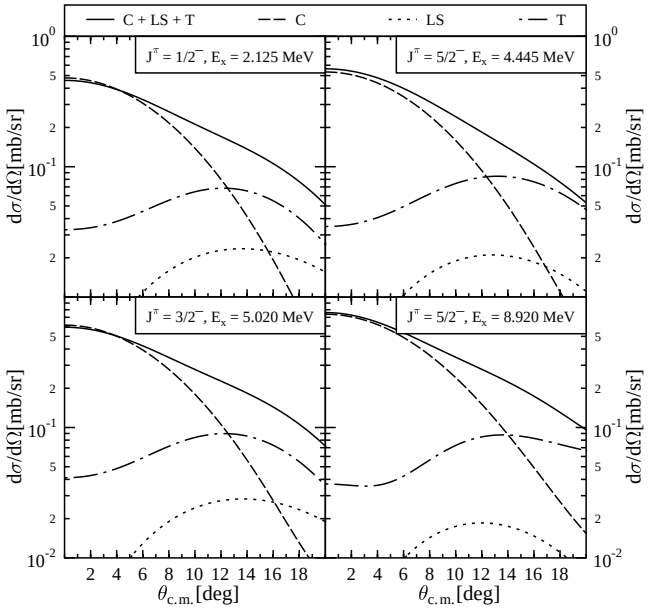

FIG. 11. Contributions of the central (C), spin-orbit (LS), and tensor (T) parts of the effective nucleon-nucleon interaction, as given by Franey and Love [36], to the total calculated $M1$ cross sections of selected negative-parity states in ^{11}B.

rapidly drop to zero at small momentum transfer q, the contribution of orbital excitations to the observed $M1$ transitions can safely be neglected at forward scattering angles (at a proton energy of 150 MeV and for excitation energies below 10 MeV a momentum transfer of $q=0.5$ fm^{-1} corresponds roughly to a scattering angle of 10°). This has been confirmed by Petrovich *et al.* [47], who compared results obtained from inelastic electron scattering to results from (p,n)-type measurements. These authors explain that transitions that proceed mainly by the orbital part of the $M1$ operator were observed with the (e,e') reaction but the corresponding transitions to analog states in the mirror nuclei have not been observed with the (p,n) reaction.

The most important parts of the effective interaction for spin-flip excitations at forward angles are the central isovector force and the isoscalar tensor part of the interaction denoted as $t_{\sigma\tau}$ and $\overline{t^T}$, respectively, see Ref. [5]. The experimentally observed cross sections are proportional to the squares of the relevant parts of the effective interaction. In the limit of zero momentum transfer, the ratio of isovector to isoscalar contributions to the transition strengths due to the nature of the interaction therefore becomes $|t_{\sigma\tau}/\overline{t^T}|^2 = |160/105|^2 = 2.3$. However, the excitation of low-lying isoscalar magnetic dipole strength through the $\overline{t^T}$ term of the effective nucleon-nucleon interaction is usually hindered by nuclear-structure effects, as has been observed in the excitation of the $J^\pi;T=1^+;0$ state relative to the $J^\pi;T=1^+;1$ state in ^{12}C at excitation energies of 12.7 and 15.1 MeV, respectively [48]. To check this for the ^{11}B case, the contributions of the central (C), spin-orbit (LS), and tensor (T) parts of the effective nucleon-nucleon interaction to the total $M1$ cross sections of some of the observed transitions have been calculated with the one-body transition densities obtained with the MK3W interaction (see Fig. 11). At forward scattering angles all of the observed transitions are dominated by the central part of the nucleon-nucleon interaction. Contributions of the tensor force are about an order of magnitude weaker for scattering angles below 5°. For the extraction of $B(M1)$ values from the present measurements at forward angles, it will therefore be assumed that the observed magnetic-dipole transitions are of purely spin-isovector nature.

TABLE VI. Results to determine the spin-isovector parts of the $M1$ strengths.

E_x (MeV)	J^π	$B(\sigma\tau_z)_{SM}$ (μ_N^2)	$\sigma_{expt}/\sigma_{\mathrm{DWBA}}$	$d\sigma/d\Omega(0°)_{expt}$ (mb/sr)	$B(\sigma\tau_z)_{expt}$ (μ_N^2)
2.125	$1/2^-$	1.17	0.30 ± 0.06	0.46 ± 0.09	0.35 ± 0.07
4.445	$5/2^-$	0.77	0.50 ± 0.10	0.55 ± 0.11	0.38 ± 0.08
5.020	$3/2^-$	0.97	0.47 ± 0.09	0.58 ± 0.12	0.46 ± 0.09
8.920	$5/2^-$	0.36	1.20 ± 0.24	0.76 ± 0.15	0.43 ± 0.09

To deduce the $M1$ transition strengths from the measured cross sections, we multiply the spin-isovector $M1$ strengths calculated from shell-model wave functions with appropriate scaling factors $\sigma_{expt}/\sigma_{\mathrm{DWBA}}$ (see Table IV) obtained from the analysis of experimental angular distributions giving

$$B(\sigma\tau_z)_{expt} = B(\sigma\tau_z)_{SM} \times \frac{\sigma_{expt}}{\sigma_{\mathrm{DWBA}}}.$$

Table VI gives an overview of the results. A comparison of the results obtained in this work to spin-isovector parts of the $M1$ strengths, which have been calculated from radiative level widths by Raghavan and Pakvasa [7], is given in Table VII and exhibits a very poor agreement between the two. There are several possible reasons for this disagreement. The extraction of $M1$ strengths from measured level widths requires the $M1/E2$ mixing ratios to be known. These are subject to rather large experimental uncertainties [49,50] or, in the case of the $J^\pi=1/2^-$ state at $E_x=2.125$ MeV, are not known at all [the $B(E2)$ value for the transition to this state has not been determined from radiative widths, but has been deduced from the ^{208}Pb(^{11}B, ^{11}B$'$) reaction [51]]. Furthermore, the calculation of the spin-isovector contributions to the total of $M1$ strengths from radiative widths is hindered by the contributions of the orbital parts of the transition operator, which cannot be neglected in these kinds of measurements. The ratio of spin and orbital contributions to the ob-

TABLE VII. Spin-isovector $M1$ strengths obtained in this work compared to results deduced from radiative widths.

E_x (MeV)	J^π	$B(\sigma\tau_z)_{expt}$ (μ_N^2)	$B(\sigma\tau_z)$ (μ_N^2)
2.125	$1/2^-$	0.35 ± 0.07	0.63 ± 0.05
4.445	$5/2^-$	0.38 ± 0.08	1.03 ± 0.10
5.020	$3/2^-$	0.46 ± 0.09	1.02 ± 0.04

[a]From Ref. [7].

TABLE VIII. Spin-isovector parts of the $M1$ strengths in ^{11}B compared to experimental analog Gamow-Teller strengths for transitions to excited states in ^{11}C.

E_x in ^{11}C (MeV)	J^π	$B(GT)^a$	$B(GT)^b$	$B(\sigma\tau_z)_{expt} \times 0.76/\mu_N^2$
2.000	$1/2^-$	0.40 ± 0.03	0.28 ± 0.06	0.27 ± 0.05
4.319	$5/2^-$	0.96 ± 0.06	0.68 ± 0.15	0.29 ± 0.06
4.804	$3/2^-$		0.37 ± 0.08	0.35 ± 0.07
8.105	$3/2^-$	0.44 ± 0.01		0.33 ± 0.07
8.420	$5/2^-$			

[a]From Ref. [12].
[b]From Ref. [13].

served transitions is estimated using shell-model wave functions. As the total of the $M1$ strengths extracted from those wave functions is for most of the states not in good agreement with the measurements (see Table I) it cannot be expected that this ratio is predicted correctly.

B. Comparison to measured Gamow-Teller strengths

In a simple picture, where effects such as MECs [15] are neglected, there is a direct relation between the spin-isovector parts of the $M1$ strength of a transition and the Gamow-Teller strength of the analog transition to the mirror nucleus [16]

$$\frac{B(GT)}{B(\sigma\tau_z)/\mu_N^2} = \frac{8\pi}{3(g_{IV}^s)^2} \frac{\langle T_i T_{zi} 1 \pm 1 | T_f T_{zf}\rangle^2}{\langle T_i T_{zi} 10 | T_f T_{zf}\rangle^2}, \quad (19)$$

with $g_{IV}^s = (g_p^s - g_n^s)/2$. Inserting the proper initial and final isospins for the states in question, this ratio becomes

$$\frac{B(GT)}{B(\sigma\tau_z)/\mu_N^2} = \frac{8\pi}{3(g_{IV}^s)^2} \frac{\langle \frac{1}{2}\ \frac{1}{2} - 1 | \frac{1}{2} - \frac{1}{2}\rangle^2}{\langle \frac{1}{2}\ \frac{1}{2} 10 | \frac{1}{2}\ \frac{1}{2}\rangle^2} \approx 0.76. \quad (20)$$

Table VIII shows a comparison of Gamow-Teller strengths to the values obtained from the above-mentioned proportionality. The states at $E_x = 4.319$ and 4.804 MeV as well as at $E_x = 8.105$ and 8.420 MeV in ^{11}C have been observed as a doublet in the experiments of Ref. [12] and combined Gamow-Teller strengths are therefore given for these states. In case of the second doublet, the complete quoted Gamow-Teller strength is attributed to the $J^\pi = 5/2^-$ state. This is confirmed by the observation that the transition to the $J^\pi = 3/2^-$ state at $E_x = 8.560$ MeV in ^{11}B, which is the analog of the $J^\pi = 3/2^-$ state of the doublet, is predominantly of $E0$ nature (see Sec. III C 1).

Figure 12 gives a graphical representation of the comparison between spin-isovector parts of the $M1$ strengths and the Gamow-Teller strengths, including the results obtained by Raghavan and Pakvasa [7]. Judging from the figure, the results of the analysis of inelastic proton scattering are in better agreement with the measured Gamow-Teller strengths than the data points extracted from radiative widths. This finding may, however, be modified by the inclusion of MEC effects.

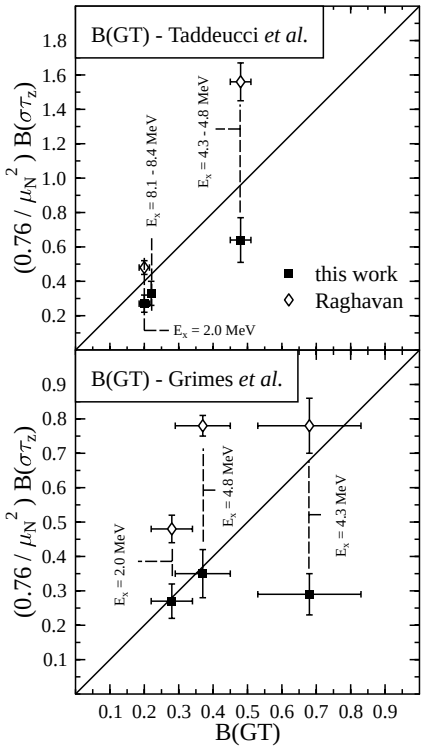

FIG. 12. Spin-isovector parts of the $M1$ strengths compared to Gamow-Teller strengths. The plots are produced using $B(GT)$ values from Ref. [12] (upper panel) and from Ref. [13] (lower panel). In the upper panel the data are summed for the states at $E_x = 4.3$ and 4.8 MeV and at $E_x = 8.1$ and 8.4 MeV to allow a comparison with Ref. [12]. See Table VIII for details.

Using relation (4) and the value of $g_A/g_V = 1.26$, the excitation strength $\lambda_{\rm NC}$ was calculated on basis of the values of $B(\sigma\tau_z)_{expt}$ as listed in Table VII. The values for $\lambda_{\rm NC}$ are 0.11 ± 0.02, 0.11 ± 0.02, and 0.14 ± 0.03, for the transitions to the states at 2.12, 4.45, and 5.02 MeV, respectively. Especially, for the last two transitions the value for $\lambda_{\rm NC}$ is much smaller than that listed by Raghavan [7], which means that the total yield per weight of boron for the important transitions to the states at 4.45 and 5.02 will be a factor of 2 smaller than that mentioned by Raghavan.

C. Extraction of $E2$ strengths

$E2$ transitions caused by electromagnetic probes proceed via the electric operator $O(EL_{M_L})$. When using free nucleon charges e_p and e_n the transition strengths for these excitations depend on single-particle matrix elements between proton states only. Hadronic probes, however, induce transitions both between proton states and between neutron states and different operators have to be used to evaluate the wave functions of initial and final states. Following Ref. [52], the operators $O(LST)$ for the four possible combinations of orbital-momentum transfer, spin transfer, and isospin transfer (see Table III), which contribute to the observed $E2$ transitions, are given by

TABLE IX. Matrix elements $\mathcal{M}(LST)$ of the observed $E2$ transitions calculated from shell-model wave functions.

E_x (MeV)	J^π	$\mathcal{M}(200)$	$\mathcal{M}(201)$	$\mathcal{M}(210)$	$\mathcal{M}(211)$
2.125	$1/2^-$	−2.394	−0.692	−1.377	1.006
4.445	$5/2^-$	−5.150	0.413	−1.130	0.674
5.020	$3/2^-$	2.538	0.826	0.219	0.027
6.743	$7/2^-$	−4.216	−1.547	0.209	−1.442
8.920	$5/2^-$	0.374	0.103	0.259	0.002

$$O(200)=\sum_{k=1}^{A} r_k^2 Y_{2M}(\hat{r}_k),$$

$$O(201)=\sum_{k=1}^{A} r_k^2 Y_{2M}(\hat{r}_k)\tau_{zk},$$

$$O(210)=\sum_{k=1}^{A} r_k^2[\vec{\sigma}_k\otimes Y_{2M}(\hat{r}_k)]_2, \tag{21}$$

$$O(211)=\sum_{k=1}^{A} r_k^2[\vec{\sigma}_k\otimes Y_{2M}(\hat{r}_k)]_2\tau_{zk}.$$

To get an insight into the importance of the different spin and isospin parts of the transitions, Table IX gives an overview of the $E2$ matrix elements $\mathcal{M}(LST)=\langle f||O(LST)||i\rangle$ of the observed states calculated from appropriate shell-model wave functions (see Sec. III B). From a comparison of the matrix elements it becomes apparent that all of the observed transitions are dominated by the isoscalar non-spin-flip contribution $\mathcal{M}(200)$. This dominance of the isoscalar non-spin-flip part is a consequence of the nature of the residual nucleon-nucleon interaction inside the nucleus. In a collective picture isovector transitions involve a motion of protons against neutrons whereas for isoscalar transitions they move in phase. The energy needed for isovector excitations that require a separation of protons and neutrons is therefore higher than that needed for isoscalar excitations [53]. Similar arguments hold for the spin part of the observed $E2$ transitions.

At a momentum transfer of $q=0.9$ fm^{-1}, which corresponds roughly to the position of the maxima of the $E2$ cross sections, the largest contributions to the effective nucleon-nucleon interaction are given by the central isoscalar non-spin-flip part and by the spin-isovector tensor component, both being approximately equally strong. Those components coupling to the isoscalar spin-flip matrix element are suppressed by a factor of 4 relative to the above-mentioned parts of the interaction and the isovector non-spin-flip contributions are more than a factor 30 weaker.

The actual transition strengths are related to the matrix elements by

$$B(E2_{ST})=\frac{\mathcal{M}(LST)^2}{2J_i+1}b^4 \tag{22}$$

TABLE X. $E2$ transition strengths calculated from shell-model wave functions.

E_x (MeV)	J^π	$B(E2_{00})$ (fm^4)	$B(E2_{00+11})$ (fm^4)
2.125	$1/2^-$	11.83	3.97
4.445	$5/2^-$	54.73	41.34
5.020	$3/2^-$	13.29	13.57
6.743	$7/2^-$	36.67	66.05
8.920	$5/2^-$	0.29	0.29

with b being the harmonic-oscillator parameter. Calculated values for the $E2$ transition strengths are displayed in Table X, where the column $B(E2_{00})$ refers to isoscalar non-spin-flip strengths and column $B(E2_{00+11})$ gives the combined transition strengths, which are obtained when also taking the spin-isovector matrix element into account.

To deduce experimental values of the $E2$ transition strengths, the calculated results are multiplied with scaling factors $\sigma_{exp}/\sigma_{\mathrm{DWBA}}$ found in the analysis of the experimental angular distributions (see Table IV). Again, values in Table XI are given either assuming that the observed $E2$ transitions are of purely isoscalar non-spin-flip nature or taking into account the spin-isovector contribution also.

V. SUMMARY AND CONCLUSION

Inelastic transitions to all known [11] positive- and negative-parity states in ^{11}B up to the $J^\pi=5/2^+$ state at an excitation energy of $E_x=9.274$ MeV have been analyzed with the exception of the $1/2^+$ state at 6.792 MeV. The extraction of parity-changing transitions has been possible due to the good energy resolution and high statistics of the experimental data and makes this the first observation of positive-parity states in ^{11}B using inelastic proton scattering.

Measured angular distributions were compared to the results of fully microscopic DWBA calculations. As ^{11}B has a nonzero ground-state spin, each transition contains at least two different multipole contributions. Calculated angular distributions for the different multipolarities of a certain transition were fitted to the experimental data, providing a set of scale factors (see Table IV) that were subsequently used to obtain experimental estimates of the corresponding electromagnetic transition strengths. Unlike the transitions to negative-parity states, which are mostly dominated by the

TABLE XI. $E2$ transition strengths extracted from calculated $B(E2_{ST})$ values and experimental scaling factors.

E_x (MeV)	J^π	$\frac{\sigma_{expt}}{\sigma_{\mathrm{DWBA}}}$	$B(E2_{00})_{expt}$ (fm^4)	$B(E2_{00+11})_{expt}$ (fm^4)
2.125	$1/2^-$	0.7±0.1	8.3±1.7	2.8±0.6
4.445	$5/2^-$	0.8±0.2	41.0±8.2	31.0±6.2
5.020	$3/2^-$	0.3±0.1	4.0±0.8	4.1±0.8
6.743	$7/2^-$	0.7±0.1	25.7±5.1	46.2±9.2
8.920	$5/2^-$	0.5±0.1	0.15±0.03	0.15±0.03

$M1$ and $E2$ contributions, the transitions to positive-parity states usually contain three relevant multipole contributions over the observed angular range. This hinders an unambiguous determination of the individual multipole contributions to these transitions and the corresponding scaling factors are therefore given in the form of ranges or upper limits. A special case is given by the transition to the negative-parity state at $E_x = 8.560$ MeV for which Ajzenberg-Selove [11] gives a tentative assignment of $J^\pi = 3/2^-$. The steep rise of the cross section towards small angles indicates that the transition is predominantly of $E0$ type, which would confirm this spin and parity assignment. The observed $E2$ transitions are predominantly of isoscalar non-spin-flip type, although the preference for one particular mode of excitation is not as clear as in the case of $M1$ transitions.

There is a marked discrepancy when spin-isovector parts of the $M1$ strengths from the analysis presented in this work are compared to results that were obtained by Raghavan and Pakvasa [7] from an analysis of radiative-width data (see Table VII). The reasons for this discrepancy are related to the model dependences inherent to the extraction of transition strengths from the different types of experimental data. The extraction of $M1$ strengths from measured level widths requires the knowledge of $M1/E2$ mixing ratios that are subject to rather large experimental uncertainties [49,50]. Also, the orbital part of the $M1$ operator cannot be neglected in measurements with electromagnetic probes. The ratio of spin and orbital contributions to the observed $M1$ strengths has therefore been estimated by Raghavan and Pakvasa [7] from shell-model calculations. Taking the isovector $M1$ strengths from the present analysis, we find that the yield for the flavor-independent detection of neutrinos using transitions to the 4.45- and 5.02-MeV states in ^{11}B will be a factor of 2 smaller as calculated by Raghavan [7].

For an independent measure of the quality of the extracted $M1$ strengths a comparison has been made to Gamow-Teller strengths that have been determined from (p,n)-type experiments [12,13]. In a simple picture, where effects such as meson-exchange currents are neglected, there is a direct relation between the spin-isovector parts of the $M1$ strength of a transition and the Gamow-Teller strength of the analog transition to the mirror nucleus [see Eq. (20)]. Judging from Fig. 12, the results of the analysis presented in this work are in better agreement with the measured Gamow-Teller strengths than the values estimated by Raghavan and Pakvasa [7].

ACKNOWLEDGMENTS

We acknowledge H. Sakai for providing the enriched ^{11}B target and A. Brown for helpful discussions on the shell-model calculations. The support of the cyclotron crew of AGOR throughout the experiment is greatly appreciated. This work was performed as part of the research program of the Stichting voor Fundamenteel Onderzoek der Materie (FOM) with financial support from the Nederlandse Organisatie voor Wetenschappelijk Onderzoek (NWO) and the Fund for Scientific Research (FSR) Flanders. It was supported by the European Community through the Human Capital and Mobility Program under Contract No. ERBCHRX-CT94-0562 and the Land Nordrhein-Westfalen. Two of us (K.A. and P.K.D.) gratefully acknowledge the support provided by a grant from the Australian Research Council.

[1] F. Osterfeld, Rev. Mod. Phys. **64**, 491 (1992).
[2] S. Raman, L.W. Fagg, and R.S. Hicks, in *Electric and Magnetic Giant Resonances in Nuclei*, edited by J. Speth (World Scientific, Singapore, 1991), p. 355.
[3] G.M. Crawley, N. Anantaraman, A. Galonsky, C. Djalali, N. Marty, M. Morlet, A. Willis, J.C. Jourdain, and P. Kitching, in *Spin Excitations in Nuclei*, edited by F. Petrovich, G.E. Brown, G.T. Garvey, C.D. Goodman, R.A. Lindgren, and W. G. Love (Plenum, New York, 1984), p. 91.
[4] D. Frekers *et al.*, Phys. Lett. B **244**, 178 (1990).
[5] W.G. Love and M.A. Franey, Phys. Rev. C **24**, 1073 (1981).
[6] R.S. Raghavan, S. Pakvasa, and B.A. Brown, Phys. Rev. Lett. **57**, 1801 (1986).
[7] R.S. Raghavan and S. Pakvasa, Phys. Rev. D **37**, 849 (1988).
[8] R.S. Raghavan, Nucl. Phys. **A478**, 779c (1988).
[9] J. Rapaport and E. Sugarbaker, Annu. Rev. Nucl. Part. Sci. **44**, 109 (1994).
[10] D. Dubbers, Nucl. Phys. **A527**, 239c (1991).
[11] F. Ajzenberg-Selove, Nucl. Phys. **A506**, 1 (1990).
[12] T.N. Taddeucci *et al.*, Phys. Rev. C **42**, 935 (1990).
[13] S.M. Grimes, J.D. Anderson, J.C. Davis, R.H. Howell, C. Wong, A.W. Carpenter, J.A. Carr, and F. Petrovich, Phys. Rev. C **31**, 1679 (1985).
[14] H.C. Lee, Nucl. Phys. **A294**, 473 (1978).
[15] J.G.L. Booten, A.G.M. van Hees, P.W.M. Glaudemans, and R. Wervelman, Phys. Rev. C **43**, 335 (1991).
[16] Y. Fujita, B.A. Brown, H. Ejiri, K. Katori, S. Mizutori, and H. Ueno, Phys. Rev. C **62**, 044314 (2000).
[17] V.M. Hannen *et al.*, Phys. Rev. C **67**, 054321 (2003), following paper.
[18] A.M. van den Berg, Nucl. Instrum. Methods Phys. Res. B **99**, 637 (1995).
[19] H.J. Wörtche, Nucl. Phys. **A687**, 321c (2001).
[20] R. Bieber *et al.*, Nucl. Instrum. Methods Phys. Res. A **457**, 12 (2001).
[21] C.E. Allgower *et al.*, Nucl. Instrum. Methods Phys. Res. A **399**, 171 (1997).
[22] H. Sakai (private communication).
[23] B. Tatischeff and A. Willis, Nucl. Phys. **A115**, 593 (1968).
[24] V. Comparat, R. Frascaria, N. Marty, M. Morlet, and A. Willis, Nucl. Phys. **A221**, 403 (1974).
[25] M. Buenerd, Phys. Rev. C **13**, 444 (1976).
[26] H.O. Meyer, P. Schwandt, W.W. Jacobs, and J.R. Hall, Phys. Rev. C **27**, 459 (1983).
[27] S. Strauch and F. Neumeyer, computer code FIT 3.0, 1996.
[28] D. Hasselgren, P.U. Renberg, O. Sundberg, and G. Tibell, Nucl. Phys. **69**, 81 (1965).

[29] P.K. Deb and K. Amos, Phys. Rev. C **62**, 024605 (2000).
[30] B. Geoffrion, N. Marty, M. Morlet, B. Tatischeff, and A. Willis, Nucl. Phys. **A116**, 209 (1968).
[31] O. Sundberg and G. Tibell, Ark. Fys. **39**, 397 (1969).
[32] K. Amos, P.J. Dortmans, H.V. von Geramb, S. Karataglidis, and J. Raynal, Adv. Nucl. Phys. **25**, 275 (2000).
[33] B.A. Brown, A. Etchegoyen, and W.D.M. Rae, computer code OXBASH, MSU version, MSUCL Report No. 524, 1988.
[34] P. Goldhammer, Rev. Mod. Phys. **35**, 40 (1963).
[35] H. de Vries, C.W. de Jager, and C. de Vries, At. Data Nucl. Data Tables **36**, 495 (1987).
[36] M.A. Franey and W.G. Love, Phys. Rev. C **31**, 488 (1985).
[37] H.V. von Geramb, in *The Interaction Between Medium Energy Nucleons in Nuclei—1982*, edited by H. O. Meyer, AIP Conf. Proc. No. 97 (AIP, New York, 1983), p. 44.
[38] K. Nakayama and W.G. Love, Phys. Rev. C **38**, 51 (1988).
[39] P.J. Dortmans and K. Amos, Phys. Rev. C **49**, 1309 (1994).
[40] P.J. Dortmans, K. Amos, and S. Karataglidis, J. Phys. G **23**, 183 (1997).
[41] D.J. Millener, D.E. Alburger, E.K. Warburton, and D.H. Wilkinson, Phys. Rev. C **26**, 1167 (1982).
[42] S. Cohen and D. Kurath, Nucl. Phys. **73**, 1 (1965).
[43] S. Karataglidis, P.J. Dortmans, K. Amos, and R. de Swiniarski, Phys. Rev. C **52**, 861 (1995).
[44] J. Raynal, computer code DWBA98, NEA Data Services, NEA-1209/005, 1998.
[45] A.A. Wolters, A.G.M. van Hees, and P.W.M. Glaudemans, Phys. Rev. C **42**, 2062 (1990).
[46] P.J. Brussaard and P.W.M. Glaudemans, *Shell-Model Applications in Nuclear Spectroscopy* (North-Holland, Amsterdam, 1977).
[47] F. Petrovich, W.G. Love, and R.J. McCarthy, Phys. Rev. C **21**, 1718 (1980).
[48] J.R. Comfort, S.M. Austin, P.T. Debevec, G.L. Moake, R.W. Finlay, and W.G. Love, Phys. Rev. C **21**, 2147 (1980).
[49] E. Spamer and H. Artus, Z. Phys. **198**, 445 (1967).
[50] P.T. Kan, G.A. Peterson, D.V. Webb, S.P. Fivozinsky, J.W. Lightbody, Jr., and S. Penner, Phys. Rev. C **11**, 323 (1975).
[51] M.P. Fewell, R.H. Spear, T.H. Zabel, and A.M. Baxter, Aust. J. Phys. **33**, 505 (1980); **37**, 239(E) (1984).
[52] M.A. Hofstee *et al.*, Nucl. Phys. **A588**, 729 (1995).
[53] G.E. Brown, *Unified Theory of Nuclear Models and Forces* (North-Holland, Amsterdam, 1967).